 Related Commentary, page 662

A simulation study of the effects of cardiac anatomy in ventricular fibrillation

Fagen Xie, Zhilin Qu, Junzhong Yang, Ali Baher, James N. Weiss, and Alan Garfinkel

University of California, Los Angeles (UCLA) Cardiovascular Research Laboratory, Departments of Medicine (Cardiology), Physiological Science, and Physiology, UCLA, Los Angeles, California, USA.

In ventricular fibrillation (VF), the principal cause of sudden cardiac death, waves of electrical excitation break up into turbulent and incoherent fragments. The causes of this breakup have been intensely debated. Breakup can be caused by fixed anatomical properties of the tissue, such as the biventricular geometry and the inherent anisotropy of cardiac conduction. However, wavebreak can also be caused purely by instabilities in wave conduction that arise from ion channel dynamics, which represent potential targets for drug action. To study the interaction between these two wave-breaking mechanisms, we used a physiologically based mathematical model of the ventricular cell, together with a realistic three-dimensional computer model of cardiac anatomy, including the distribution of fiber angles throughout the myocardium. We find that dynamical instabilities remain a major cause of the wavebreak that drives VF, even in an anatomically realistic heart. With cell physiology in its usual operating regime, dynamics and anatomical features interact to promote wavebreak and VF. However, if dynamical instability is reduced, for example by modeling of certain pharmacologic interventions, electrical waves do not break up into fibrillation, despite anatomical complexity. Thus, interventions that promote dynamical wave stability show promise as an antifibrillatory strategy in this more realistic setting.

Introduction

In the normal heart, the wave of electrical activation that triggers synchronized contraction moves in a roughly planar fashion through the ventricular myocardium. In ventricular fibrillation (VF), the most common cause of death from cardiovascular disease, this electrical wave breaks up into multiple wavelets that meander chaotically through the myocardium (1–7), precluding the coordinated contraction that is necessary to maintain blood pressure.

This "electrical turbulence" is initiated and maintained by the process of wavebreak, in which new waves are continually generated to replace those that are extinguished because of encounters with each other or with refractory tissue. Traditionally, many cardiac researchers believed that wavebreak was due to external obstacles and focused on the role of anatomical and/or electrophysiological heterogeneities and obstacles, such as built-in gradients of electrophysiological properties, or the presence of infarction, ischemia, and/or fibrosis as the primary causes of wavebreak. However, dynamicists discovered that purely dynamical instabilities, arising from cellular properties such as ion channel dynamics, can also cause wavebreak even in perfectly homogeneous tissue.

What drives fibrillation: fixed heterogeneities, dynamical instabilities, or a synergistic interaction between the two? The answer is controversial, because both factors are inevitably present in real cardiac tissue. Indeed, even in normal cardiac tissue without significant fibrosis, infarction, or ischemia, VF can be induced by a sufficiently large electrical stimulus, and it is still unclear what factors cause wavebreak. For example, one important aspect of the gross anatomy of the heart is the shape of the ventricular cavities, the interventricular septum, and the overall geometry of the lower heart (8). Another critical aspect of cardiac gross anatomy is the anisotropy of electrical conduction, which is created by the twisted distribution of cardiac fibers through the myocardial wall (9). This "fiber twist" can play a role in creating wavebreak, as has been shown in models of 3D rectangular slabs of tissue (10, 11). In addition to these fixed factors, one of the key dynamical factors that cause wavebreak is electrical restitution. After an action potential, the cardiac cell must recover ionic balance and replenish calcium stores in the sarcoplasmic reticulum. Ion channels (Na^+, K^+, or Ca^{++}), having been inactivated or deactivated, must recover to their resting state. These restorative processes take place during the electrical diastolic interval (DI), the interval between repolarization and the next action potential upstroke. Physiologically, it is important for the action potential duration (APD) to shorten as the DI decreases, to preserve diastolic filling time and coronary flow as the heart rate increases. Thus, the ion channel recovery processes mentioned above are tailored to accomplish this, producing the phenomenon known as APD restitution. APD restitution quantifies the relationship between APD and DI, and when APD is plotted as a function of the previous DI, the result is called the APD restitution curve (see also supplemental material; available at http://www.jci.org/cgi/content/full/1113/5/686/DC1). Another important type of restitution is of conduction velocity: if the DI is too short, Na^+ channels have not fully recovered from inactivation, and so propagation of the following depolarization wave is slowed. Both forms of restitution are important in the genesis of VF (12).

The APD restitution curve has an immediate dynamical consequence for wave stability. Suppose a cell is being paced at a constant slow rate. Since the rate is slow, the DI will be long, the cell will fully recover, and the following APD will be the same as the first. But as rate is increased, the DI shortens, and the cell will not be completely recovered at the next stimulus. This makes the following action potential shorter. But then the *next* DI will be longer, and in this way, complex oscillations of APD can be generated by rapid pacing and a sufficiently steep APD restitution curve (13). (See also supplemental material).

Nonstandard abbreviations used: action potential duration (APD); diastolic interval (DI); left ventricle (LV); Luo-Rudy phase 1 (LR1); right ventricle (RV); two-dimensional (2D); ventricular fibrillation (VF).

Conflict of interest: The authors have declared that no conflict of interest exists.

Citation for this article: *J. Clin. Invest.* **113**:686–693 (2004). doi:10.1172/JCI200417341.

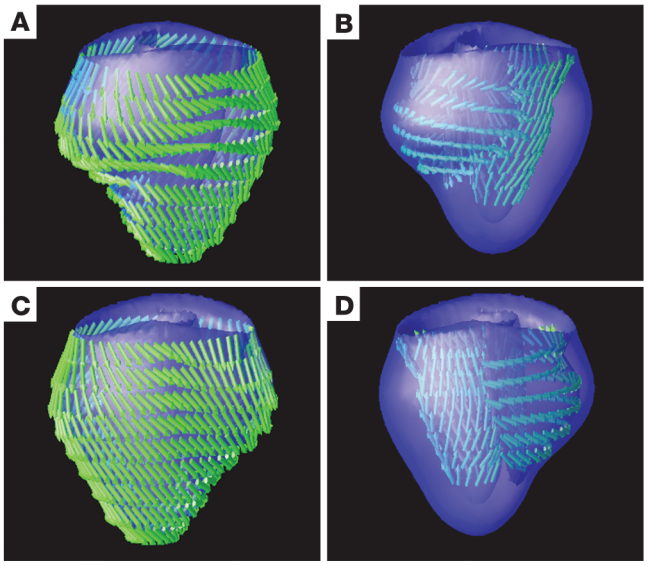

Figure 1
Front view (**A** and **B**) and back view (**C** and **D**) of canine ventricular anatomy and fiber vectors on the epicardium and endocardium. The green arrows represent fiber direction. The grid size is $359 \times 275 \times 253$ nodes, corresponding to a physical size of $8.975 \times 6.875 \times 6.325$ cm^3.

Dynamicists conjectured, and showed in simulations, that this same instability could cause wavebreak, and hence serve as the dynamical engine that drives wavebreak (14). In simulations of cardiac tissue, if the slope of the APD restitution curve (APD_{n+1} vs. DI_n) is steep (>1) over a sufficiently wide range of DIs, then wavebreak quickly leads to a complex, multi-wavelet, VF-like state. Although electrical restitution is not the only factor that creates dynamical wave instability, strategies aimed at altering electrical restitution have shown promise against VF in computer simulations (11, 14–16) and, most importantly, in real cardiac tissue (5, 6).

These dynamical instabilities interact synergistically with fixed heterogeneities to facilitate wavebreak. In computational studies in 3D rectangular slabs, some waves that remain intact in homogeneous tissue can break up into a fibrillation-like state when anisotropic conduction is introduced (11, 17, 18). It is therefore unclear how important ventricular geometry and anisotropic conduction are in generating wavebreak. The recent availability of an anatomically realistic computer model of the ventricles, coupled with an ionic model of the cardiac action potential, provides an opportunity to examine the role of cardiac anatomical properties in perpetuating VF. We find that the steepness of the APD restitution slope remains a major determinant of wave instability in the anatomical heart, but that the threshold of steepness required to induce wave breakup is significantly reduced by anatomical features, such as the ventricular cavities, and by the presence of anisotropic conduction, which causes waves to fold and drift.

Methods

Mathematical model. A mathematical model of cardiac conduction begins with a model of the cardiac cell. We used the Luo-Rudy phase 1 (LR1) ventricular cell model (19), with some of its parameters modified to fit the canine action potential (see supplemental material for details). This model contains an Na^+ current, I_{Na}; a slow inward (L-type) Ca^{++} current, I_{si}; a time-dependent K^+ current, I_K; a time-independent K^+ current, I_{K1}; a plateau K^+ current, I_{Kp}; and a background current, I_b. Each of the ionic currents has the form

Equation 1

$$I_Y = G_Y \times Z_1 \times Z_2 \times (V - V_Y)$$

where V is the cellular transmembrane potential and Y ranges over Na, K, Ca, etc. G_Y is the maximal value of the channel conductance (and therefore reflects channel density in the cell as well as channel function). Z_1 and Z_2 are gate variables, typically voltage- and/or ion-dependent, and V_Y is the reversal potential for the ion channel in question. We used G_{si}, the maximal value of the slow inward L-type calcium current (and the target of calcium channel blockers), as our control parameter to alter restitution properties.

A tissue-conduction model is then created by coupling of cells to each other in a 3D lattice with current diffusing from one cell to its neighbors through gap junctions, represented as ohmic resistors. This gives rise to a partial differential equation,

Equation 2

$$\partial_t V = -I_{ion}/C_m + \nabla \cdot \tilde{D} \nabla V$$

where V is the cellular transmembrane potential, $C_m = 1$ μF/cm^2 is the capacitance, and $\tilde{D}$ is the 3×3 diffusion tensor (see supplemental material). I_{ion} is the total ionic current density from the LR1 ventricular cell model.

Anatomy of canine ventricles. Equation 2, representing tissue conduction, is then placed in the geometry of the canine heart. For this purpose, we used canine anatomy and fiber-orientation data obtained from the Cardiac Mechanics Research Group at the University of California, San Diego (San Diego, California, USA). Our visualization of the resulting structures, including the left ventricle (LV), right ventricle (RV), and fiber vectors on the epicardium and endocardium, is shown in Figure 1, in anterior (Figure 1, A and B) and posterior views (Figure 1, C and D).

Our numerical methods are described in detail in the supplemental material. With these methods, we were able to simulate 1 second of our model in about 2 hours using thirty 1.4-GHz processors in parallel.

Results

APD restitution and spiral wave dynamics in two-dimensional homogeneous cardiac tissue. In two dimensions, cardiac reentry that is not constrained by anatomically defined pathways will take the form of a spiral wave (20, 21). Both in simulations (22) and in real hearts (5), one of the most effective means to flatten APD restitution slope is to block the Ca^{++} current amplitude. In the LR1 ventricular action potential model, four distinct phenotypes of spiral wave reentry can be generated by variation of G_{si}, the parameter that controls Ca^{++} current amplitude: stable (periodic) rotation, quasiperiodic ("weak") meander, chaotic ("strong") meander (or "hypermeander"), and spiral wave breakup (11, 16). In two-dimensional (2D) homogeneous tissue, a spiral wave is nearly stable when $G_{si} = 0$ μA/cm^2 (Figure 2A), displays quasiperiodic meander when $G_{si} = 0.025$ μA/cm^2 (Figure 2B), and displays chaotic hypermeander when $G_{si} = 0.045$ μA/cm^2 (Figure 2C) and $G_{si} = 0.060$ μA/cm^2 (Figure 2D). Beyond $G_{si} \approx 0.065$ μA/cm^2, spontaneous spiral wave breakup occurs (not shown). The Ca^{++} current modifications that produce these distinct spiral wave

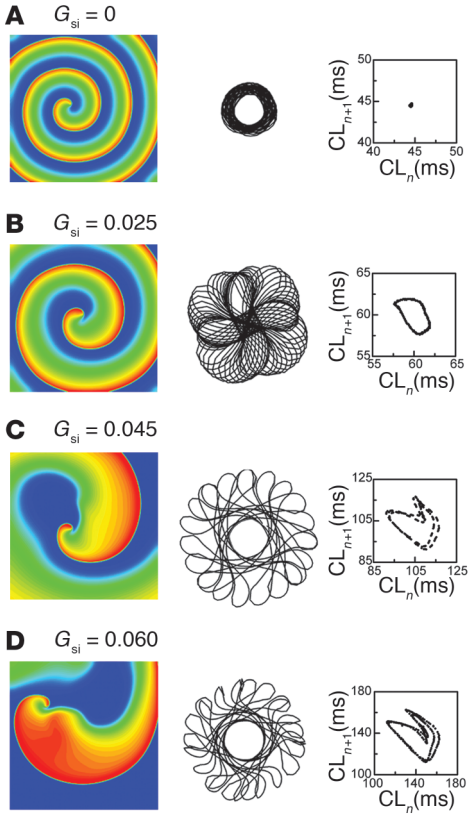

Figure 2
Spiral wave behaviors as a function of the maximum conductance of the slow inward calcium current (G_{si}) in homogeneous isotropic 2D cardiac tissue (10 × 10 cm²). (**A**–**D**) Nearly stable (G_{si} = 0), weak meander (G_{si} = 0.025 μA/cm²), and strong meander (G_{si} = 0.045 and 0.060 μA/cm²). Left: Voltage snapshots at steady state. Red represents depolarized tissue at the wavefront, while blue represents repolarized tissue at the waveback. Middle: Trajectory of the spiral wave tip. Right: Return map of successive cycle lengths (CL_n) of the spiral wave.

behaviors progressively increase the slope of the APD restitution curve (Figure 3). Note that the slope of the APD restitution curve at short DIs was greater than 1 for the strong-meander cases (shown in Figure 2, C and D), while for the stable and weak-meander cases (Figure 2, A and B) the slope was less than 1 everywhere.

Effects of 3D ventricular anatomy on scroll wave activities. To examine the effects of ventricular gross anatomy alone on electrical wave propagation, we introduced the four spiral wave phenotypes described above into the anatomical canine ventricular model, in which conduction was made isotropic. In 3D, the equivalent of a spiral wave is a scroll wave, which may be thought of as a stack of 2D spiral waves united by a line joining the spiral wave tips. This line is called the filament of the scroll. At G_{si} = 0 (which generated a nearly stationary spiral wave in 2D), an initiated scroll wave (see supplemental Methods) remained intact and nearly stable (Figure 4A). Its filament was straight and separated into two parts on either side of the LV cavity. The motion of the filament tip on the epicardium traced a circular pattern, confirming that the scroll wave was stable. The cycle length of the scroll wave was constant at 44.7 ms, nearly equal to that of the 2D spiral wave (Supplemental Table 1).

For a spiral wave that weakly meandered in 2D (G_{si} = 0.025 μA/cm²), the corresponding scroll wave in 3D also remained intact and continued to meander weakly (Figure 4B). Its meander was characterized by a "flower pattern" of the filament-tip trajectory on the epicardium. Thus the anatomical structure did not have a significant effect on the scroll wave filament, which remained nearly straight. The average cycle length (60.4 ms) of the scroll wave was also near that of its 2D spiral wave analog (see Supplemental Table 1).

For a spiral wave that strongly meandered in 2D (G_{si} = 0.045 μA/cm²), the corresponding 3D scroll wave also remained intact, but the initially straight filament became twisted, and the waves displayed large irregular spatial oscillations (Figure 4C). The filament tip on the epicardium traced complicated irregular patterns, reflecting the interaction of the dynamical instability with the anatomy of the ventricle.

When G_{si} was increased beyond 0.055 μA/cm² (corresponding to an even more strongly meandering spiral wave in 2D, but not yet at the threshold for breakup in 2D), the corresponding 3D scroll wave now broke up after several rotations into complex multiple wavelets, producing a fibrillation-like state (Figure 4D). Thus, the interaction of the dynamical instability with the gross anatomy alone, even without anisotropic conduction, caused the G_{si} threshold for breakup to be reduced from 0.065 to 0.055 μA/cm².

Nonlinear dynamics of scroll waves. Nonlinear dynamics distinguishes several different qualitative forms of behavior. Strictly periodic behavior is the simplest form of time-varying behavior; more complex behaviors include quasiperiodicity (exhibiting several independent frequencies) and deterministic chaos (characterized by aperiodic, irregular behavior). In a number of model systems, mathematical and real, this sequence of behaviors can be produced by one and the same system as a single critical parameter is varied (23). In our model, exactly such a sequence was produced by an increase in G_{si}. The distinct scroll wave phenotypes gave rise to these distinct patterns, as seen in the time series of electrical activity recorded at a representative point in the tissue. The voltage record displayed strictly periodic behavior at G_{si} = 0 (stable scroll wave), quasiperiodicity at G_{si} = 0.025 μA/cm² (weakly meandering scroll wave), and chaos at both G_{si} = 0.045 μA/cm² (strongly meandering scroll wave) and G_{si} = 0.060 μA/cm² (scroll wave breakup). Corresponding to these voltage traces, we also plotted cycle-length return maps (CL_{n+1} vs. CL_n). The single fixed point in the cycle-length return map in Figure 5A shows that the dynamics were stable (that is, periodic), and the ring or circle in Figure 5B shows that the dynamical behavior was quasiperiodic, while the fuzzy ring in Figure 5C and the irregular complex pattern in Figure 5D are characteristic of chaotic behavior.

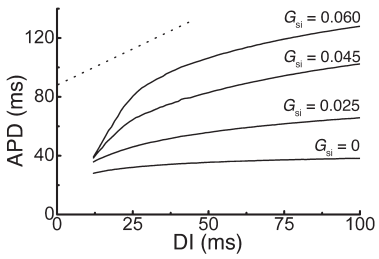

Figure 3
APD restitution curves, obtained in a one-dimensional ring of cells, as a function of G_{si} for the different spiral wave regimes corresponding to G_{si} = 0 (nearly stable), G_{si} = 0.025 μA/cm² (weak meander), and G_{si} = 0.045 and 0.060 μA/cm² (strong meander). The dotted line has slope 1.

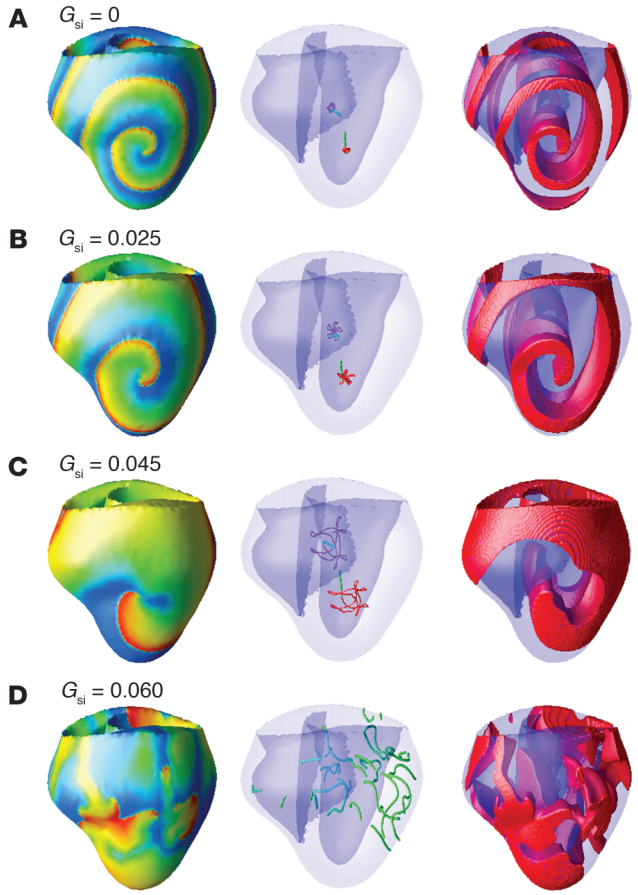

Figure 4
Scroll wave dynamics in canine ventricular geometry with homogeneous and isotropic tissue, for APD restitution curves corresponding to those in Figure 3. (**A**) G_{si} = 0, showing stable scroll waves. (**B**) G_{si} = 0.025 μA/cm², showing weakly meandering scroll waves. (**C**) G_{si} = 0.045 μA/cm², showing strongly meandering scroll waves. (**D**) G_{si} = 0.060 μA/cm², illustrating scroll wave breakup. (**A**–**D**) Left: Snapshots of voltage on the surface (red, depolarized; blue, repolarized). Middle: Filaments of scroll wave reentry and tip trajectories of reentry on the epicardium. Right: Snapshots of isosurfaces of voltage (V = –30 mV). Video of the corresponding scroll waves is provided as supplemental data.

3D ventricular anatomy with anisotropy. We next added anisotropic conduction with physiological fiber rotation to the anatomical ventricular model and examined its effects on scroll wave dynamics. For a stable spiral wave in 2D (G_{si} = 0), the corresponding scroll wave in 3D remained intact, but now its filament became somewhat folded and twisted, because of the fiber rotation, and its wave tip on the epicardium traced a meandering, rather than circular, path (Figure 6A). The average cycle length of the scroll wave was about 45.5 ms, nearly the same as in the 2D and the 3D homogeneous cases (Supplemental Table 1).

For a weakly meandering spiral wave (G_{si} = 0.025 μA/cm²), the corresponding scroll wave filament folded enough to cause the wave*front* to break through the epicardium (Figure 6B), but the twisted filament itself remained intact, avoiding contact with the surface, and hence avoiding being broken as a result of surface contact. The scroll wave tip on the epicardium meandered widely. The average cycle length was 60.5 ms, again about the same as in the 2D spiral wave case (Supplemental Table 1).

For a strongly meandering spiral wave (G_{si} = 0.045 μA/cm²), however, the corresponding scroll wave quickly broke up into unstable multiple wavelets, after approximately 1 second or about seven rotations (Figure 6C). Ongoing generation and annihilation of wavelets maintained the complex VF-like state.

The succession of scroll wave phenotypes could also be seen in the virtual ECG. As G_{si} was increased from 0 (the stable case) to 0.025 μA/cm² (the weak-meander case) or to 0.045 μA/cm² (the scroll wave breakup case), the virtual ECG changed from monomorphic tachycardia (Figure 7A) to torsades de pointes–like or polymorphic tachycardia (Figure 7B) and then to VF (Figure 7C), respectively. Hence the four principal types of reentrant ventricular arrhythmias (monomorphic ventricular tachycardia, torsades de pointes, polymorphic ventricular tachycardia, and VF) were reproduced by the alteration of a single parameter, G_{si}.

In the strong-meander regime, the average cycle lengths were significantly shorter than that of the corresponding 2D spiral wave (Supplemental Table 1). This shortening of cycle length shifted the system into the very steep part of the APD restitution curve, causing large oscillations, which in turn induced wavebreak.

Structure of VF. As VF evolved from the initial reentrant wave, the number of filaments (that is, the number of independent wavelets) grew with time. In the first second or so, the number of filaments saturated, with a much larger number in the LV than in the RV (Figure 8A). Although the LV had about three times as many filaments as the

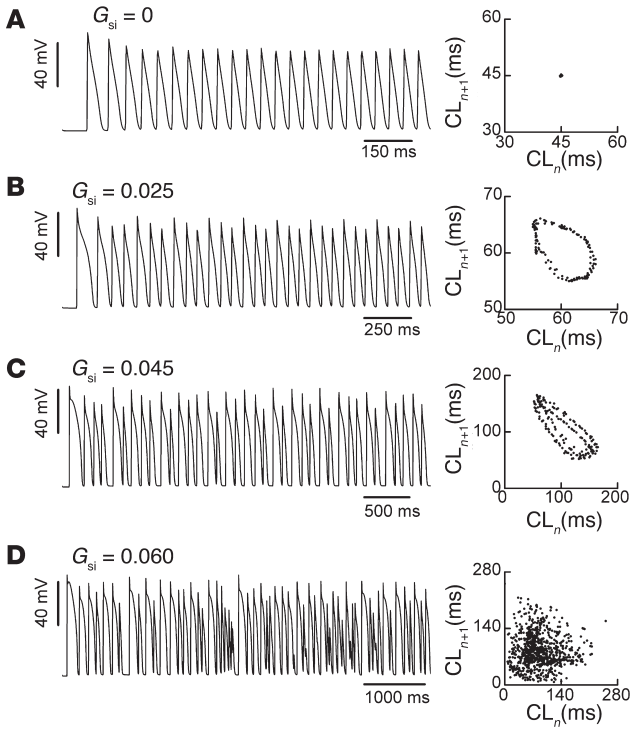

Figure 5
Action potential records (left) and return maps of successive cycle-length intervals of scroll waves (right), corresponding to the four sets of parameters in Figure 4. (**A**) G_{si} = 0, stable scroll waves. (**B**) G_{si} = 0.025 μA/cm², weakly meandering scroll waves. (**C**) G_{si} = 0.045 μA/cm², strongly meandering scroll waves. (**D**) G_{si} = 0.060 μA/cm², scroll wave breakup.

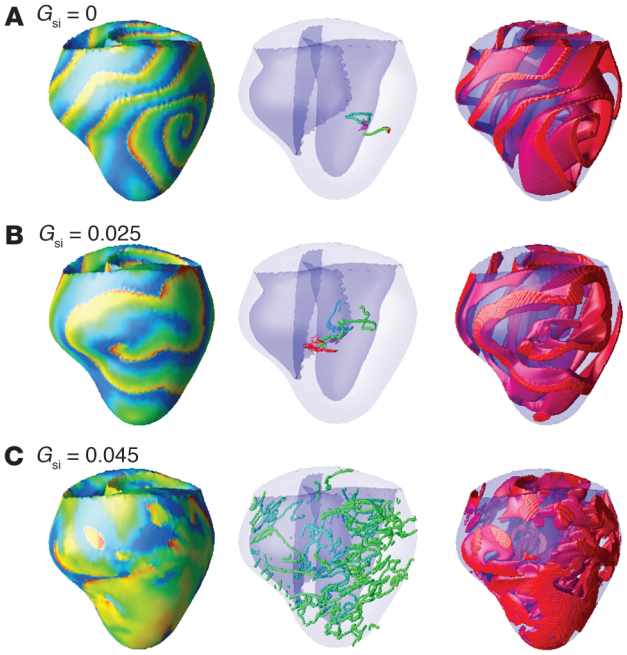

Figure 6
Scroll wave dynamical behaviors in the anatomical model of canine ventricles with fiber rotation, corresponding to the APD restitution curves in Figure 3. (**A**) G_{si} = 0; (**B**) G_{si} = 0.025 μA/cm²; (**C**) G_{si} = 0.045 μA/cm². Details are as in Figure 4. Video of the corresponding scroll waves is provided as supplemental data.

RV, it also contained about three times the volume, so filament density did not differ significantly between LV and RV (Supplemental Table 2), or between base and septum (Figure 8B and Supplemental Table 2).

The statistics of VF in our model can be compared with those of VF seen in a pig RV preparation (4). Since the experimenter can see filaments or wavebreaks only on the epi- and endocardial surfaces of the whole ventricle, we analyzed the number of surface wavebreaks in our model. During VF, there were 1.6 ± 1.0 and 2.0 ± 1.2 wavelets per mapping area (3 cm × 3 cm) in 1 second in the RV endocardium and epicardium, respectively. For comparison, for an equivalent mapping area in pig RV, experimenters reported 2.9 ± 2.8 and 2.5 ± 2.1 wavelets in 1 second on the endocardial surface and the epicardial surface, respectively. The higher density of wavelets in real heart is probably due to the presence of additional electroanatomical heterogeneities in real heart, or additional dynamical factors promoting dynamical wave instability (e.g., intracellular Ca^{++} cycling). Other wavebreak statistics from our model were also similar to experimental values (Supplemental Table 3), except for two features. First, our non-reentrant wavelets had longer lifespans (probably related to the observation above that there are fewer wavelets, hence fewer opportunities for extinction). Second, in the real heart, experimenters reported roughly twice as many wavelets completing a full 360° reentrant cycle on the endocardium as we did, although our findings on the epicardium were equivalent. This observed excess of true 360° reentry in the real endocardium may be attributable to trabeculations in the real RV endocardium, which has been shown to "anchor" waves and stabilize reentry (24).

Finally, we calculated APD restitution curves during the various types of reentry, to test whether slopes could still be accurately estimated. During VF, APD restitution curves were multivalued but still had slopes greater than 1 when best fit to a single exponential (Figure 9).

Discussion

This study investigated the relative roles of fixed factors (gross and microscopic cardiac anatomy) versus dynamical electrophysiological factors in the genesis and maintenance of wavebreak during simulated VF. Using a computer model of the canine heart and a physiologically based mathematical model of the ventricular action potential, we varied an electrophysiological parameter that has been shown in both simulation and experiment to affect dynamical wave stability by altering the steepness of the APD restitution slope. We found that while cardiac gross anatomy and fiber-angle distribution can critically influence wave stability and promote wavebreak, it is also possible to prevent wavebreak under these conditions by sufficiently reducing the slope of APD restitution.

APD restitution–driven wavebreak was augmented by "3D reentry" (11), in which large excitable gaps at one level of the tissue become vulnerable to vertical reentry by excitation wavefronts that lie immediately above or below the excitable gap and that have been slightly retarded by the different anisotropy at that level. We also saw numerous incidents of filament bending that led to breaking of the filament by contact with surfaces, confirming a theoretical conjecture (11, 17, 18).

These dynamically modifiable factors represent a new class of therapeutic targets for antifibrillatory drug action. New targets are urgently needed, since, with the exception of β-blockers, antiarrhythmic drugs have provided no consistent mortality benefit in large clinical trials and have often caused harm (25, 26).

In this study, we used the maximum conductance of the Ca^{++} current, G_{si}, to control dynamical wave stability through APD restitution slope. Lowering the value of G_{si} flattened APD restitution slope, increased dynamical wave stability, and prevented wavebreak. These findings are consistent with experimental observations, which showed that blockade of the L-type Ca^{++} current with verapamil (5) or D600 (27) also stabilized reentry and abolished VF despite physiological levels of anatomical and electrophysiological heterogeneity present in the normal ventricular tissue. Whether the same powerful anti-VF effect of flattening APD restitution slope will also occur in diseased ventricular tissue, in which both anatomical and

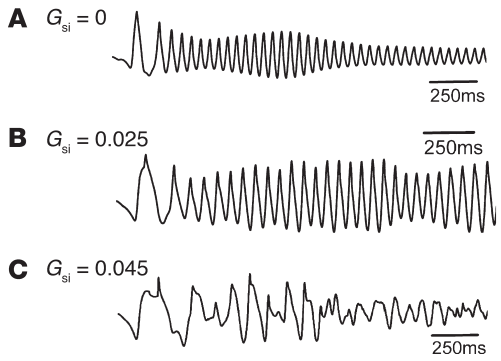

Figure 7
The virtual ECG for the scroll wave reentries shown in Figure 6. (**A**–**C**) Virtual ECGs for G_{si} = 0, G_{si} = 0.025, and G_{si} = 0.045 μA/cm², respectively. As APD restitution becomes flattened, the virtual ECG changes from monomorphic tachycardia (**A**) to a polymorphic/torsades de pointes pattern (**B**) to VF (**C**).

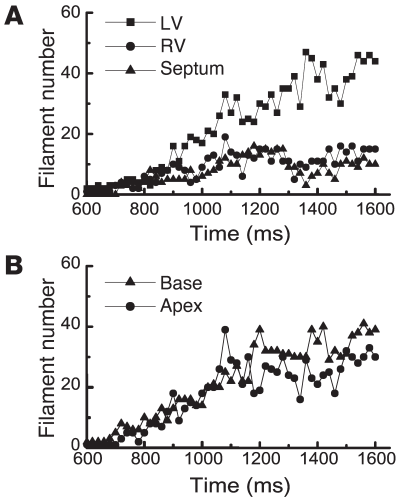

Figure 8
Evolution of filament number with time in various regions of the ventricle. (**A**) The LV evolves a larger number of filaments than does the RV or septum. (**B**) Base and apex evolve equal numbers of filaments.

electrophysiological heterogeneity are increased as a result of remodeling, is currently unknown and needs to be tested.

Blocking the L-type Ca^{++} current to prevent VF, however, is not a clinically feasible strategy, since the degree of blockade required to flatten APD restitution slope (>30%) markedly impairs excitation-contraction coupling (5). In addition, blocking the L-type Ca^{++} current to the extent required markedly shortens APD. The latter effect is not likely the cause of its antifibrillatory action, however, since other drugs that flatten APD restitution slope but prolong APD, such as bretylium, are similarly effective at preventing VF in normal heart (6). Also, simulations have demonstrated that the flattening of APD restitution slope by blocking of the Ca^{++} current remains antifibrillatory even when APD shortening is prevented by adjustment of other currents (22). Importantly, dynamical analysis has shown that it is not the amplitude of the Ca^{++} current per se that controls APD restitution slope, but rather its kinetics of recovery from inactivation (22, 28). Thus, if L-type Ca^{++} channel kinetics could be selectively modified to flatten APD restitution slope without significantly altering Ca^{++} current amplitude, this might be a clinically feasible approach to increase dynamical wave stability without impairing normal excitation-contraction coupling and contractility. Other possibilities include flattening APD restitution slope by modifying other ionic currents such as K^+ currents (26) and targeting other factors that influence dynamical wave stability, such as cardiac memory (29) and intracellular Ca^{++} cycling (30–32).

Finally, it is interesting to note that a steepening of APD restitution slope has been associated with increased VF risk. For example, a significant increase in APD restitution slope has been observed in animal models of heart failure (33, 34) and may, along with tissue remodeling, contribute to increased VF risk. β-Adrenergic stimulation also increases APD restitution slope in the human ventricle (35), which may in part contribute to the efficacy of β-blockers at reducing VF risk. It is interesting to note in this regard that β-adrenergic stimulation increases Ca^{++} channel conductance (36), so our method of increasing G_{si} may be a valid model of increased adrenergic activity in disease. APD restitution slope has also been reported to be increased in genetic (37, 38) and drug-induced models of long QT syndrome (39), for which β-adrenergic blockade is also standard therapy.

Limitations. This study has a number of limitations and should be viewed as a step in a graded sequence of experiments *in silico*, in which aspects of anatomical and cellular complexity are added one by one to test their contributions to electrical stability and instability. A number of important factors are not included in our model and represent directions for future research.

Cell model (especially intracellular calcium). Although the LR1 is an electrophysiologically based ventricular cell model, it is not complete, since it lacks the full complement of time-dependent K^+ currents and, especially, detailed intracellular Ca^{++} dynamics. The latter may be very important for cardiac arrhythmias, since intracellular Ca^{++} cycling is thought to be an independent factor influencing dynamical wave stability (30–32, 40). We did not include these further details here because, unlike in the LR1 model, the determinants of dynamical wave stability are not yet fully understood in these more detailed models. In addition, none of the models with detailed Ca^{++} dynamics was designed to operate at very rapid heart rates relevant to VF, and none has been shown to produce physiologically correct behavior under these conditions (41). The development of valid intracellular Ca^{++} dynamics at such fast heart rates remains a challenge to cardiac modelers.

Laminar sheet structure. Anatomical investigations have revealed that the transmural anatomy of the myocardium is broken by laminar sheets of nonconducting connective tissue (42). These sheets significantly slow electrical conduction across them (43). We have not attempted to include this feature in the present model, but their effect can be conjectured. In general, slowed conduction favors the genesis and maintenance of reentrant arrhythmias, since it is roughly equivalent to increasing tissue size. However, we have shown that if electrical dynamics are sufficiently stable, even grossly thickened tissue does not promote reentry (44). Therefore, we would not expect anisotropically slowed conduction to qualitatively affect our findings.

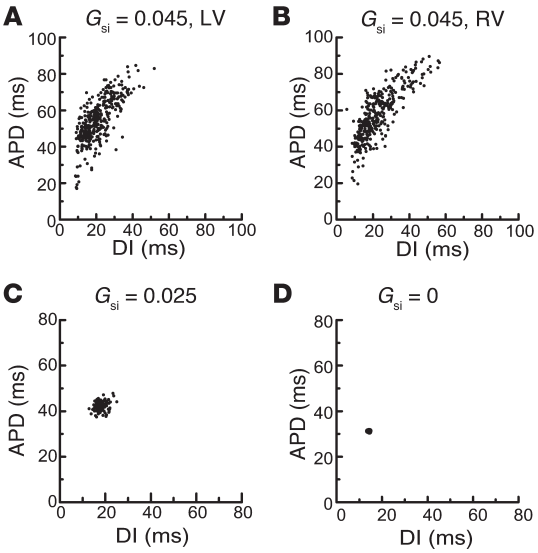

Figure 9
Restitution curves during arrhythmias of various kinds, calculated from ongoing data during arrhythmia. (**A**) VF (in LV). (**B**) VF (in RV). (**C**) Intact meandering scroll wave. (**D**) Intact stable scroll wave. DI is defined as V < –72; APD is defined as V ≥ –72.

Cardiac contraction. As the heart contracts, its electrophysiological properties will change. Obviously, contraction creates a smaller tissue size, which would have significant effects on reentrant conduction. In addition, contraction of a generic elastic excitable medium has been shown to induce vortex drift (45), which will further complicate reentrant dynamics. Finally mechanoelectrical feedback, for example through stretch-activated ion channels (46), is another important factor in the contracting heart. Incorporating these contraction effects is a challenge for further research.

Heterogeneity. Other sources of heterogeneity in real ventricle are the transmural gradients in electrophysiology, especially the epicardial/M-cell/endocardial gradient (47) and the apex-base electrophysiological gradients (3). We did not include these gradients in the present model, because their global structure and distribution in the 3D ventricular anatomy are controversial. However, we did undertake a preliminary study in a rectangular 3D slab that was a "sandwich" of the three cell types and found that the steeper restitution curves of M cells can have a somewhat proarrhythmic effect (see supplemental material). These differences can also be very important in the *initiation* of VF, for example due to "phase II reentry" (48).

We also did not include the His-Purkinje system in our model. While it is essential for normal conduction, it is not likely to play a role in the fast rates of these arrhythmias, and in fact, ablation of the His-Purkinje system was found to have no effect on VF (2).

Finally, it is known that disease processes and drugs can enhance fixed anatomical and electrophysiological heterogeneities (49). In these instances, it is possible that tissue heterogeneities play a greater role than they do in the normal ventricle simulated in our studies. This will be critical to evaluate in future studies, since this is the setting in which VF risk increases. Despite these limitations, our findings support experimental evidence that flattening of APD restitution slope has antifibrillatory effects in normal canine and porcine ventricles (5, 6) and lead to the encouraging possibility that reduction of dynamical wave instability (50) may have merit as an antifibrillatory strategy in the diseased heart as well.

Acknowledgments

This work was supported by NIH Specialized Center of Research grant P50 HL52319 and by the Laubisch and Kawata Endowments. We are grateful to Andrew McCulloch of the National Biomedical Computation Resource at the University of California, San Diego, for the anatomy and fiber vectors of the canine ventricles. We thank Paul Hoffman, Joan Slottow, and T.V. Singh of UCLA Academic Technology Services and Jong R. Kil for helpful conversations and technical assistance.

Received for publication November 7, 2002, and accepted in revised form December 16, 2003.

Address correspondence to: Alan Garfinkel, Division of Cardiology, 47-123 Center for the Health Sciences, Los Angeles, California 90095-1679, USA. Phone: (310) 794-7214; Fax: (310) 206-9133; E-mail: agarfinkel@mednet.ucla.edu.

1. Winfree, A.T. 1994. Electrical turbulence in three-dimensional heart muscle. *Science.* **266**:1003–1006.
2. Lee, J.J., et al. 1996. Reentrant wave fronts in Wiggers' stage II ventricular fibrillation: characteristics, and mechanisms of termination and spontaneous regeneration. *Circ. Res.* **78**:660–675.
3. Choi, B.R., Liu, T., and Salama, G. 2001. The distribution of refractory periods influences the dynamics of ventricular fibrillation. *Circ. Res.* **88**:E49–E58.
4. Valderrabano, M., et al. 2002. Frequency analysis of ventricular fibrillation in swine ventricles. *Circ. Res.* **90**:213–222.
5. Riccio, M.L., Koller, M.L., and Gilmour, R.F., Jr. 1999. Electrical restitution and spatiotemporal organization during ventricular fibrillation. *Circ. Res.* **84**:955–963.
6. Garfinkel, A., et al. 2000. Preventing ventricular fibrillation by flattening cardiac restitution. *Proc. Natl. Acad. Sci. U. S. A.* **97**:6061–6066.
7. Gray, R.A., Pertsov, A.M., and Jalife, J. 1998. Spatial and temporal organization during cardiac fibrillation. *Nature.* **392**:75–78.
8. Rogers, J.M. 2002. Wave front fragmentation due to ventricular geometry in a model of the rabbit heart. *Chaos.* **12**:779–787.
9. Nielsen, P.M.F., Grice, I.J.L., Smaill, B.H., and Hunter, P.J. 1991. Mathematical model of geometry and fibrous structure of the heart. *Am. J. Physiol.* **260**:H1365–H1378.
10. Fenton, F., and Karma, A. 1998. Fiber-rotation-induced vortex turbulence in thick myocardium. *Phys. Rev. Lett.* **81**:481–484.
11. Qu, Z.L., Kil, K., Xie, F.G., Garfinkel, A., and Weiss, J.N. 2000. Scroll wave dynamics in a three-dimensional cardiac tissue model: roles of restitution, thickness, and fiber rotation. *Biophys. J.* **78**:2761–2775.
12. Chen, P.S., et al. 2003. A tale of two fibrillations. *Circulation.* **108**:2298–2303.
13. Nolasco, J.B., and Dahlen, R.W. 1968. A graphic method for the study of alternation in cardiac action potentials. *J. Appl. Physiol.* **25**:191–196.
14. Karma, A. 1994. Electrical alternans and spiral wave breakup in cardiac tissue. *Chaos.* **4**:461–472.
15. Courtemanche, M., and Winfree, A.T. 1991. Reentrant rotating waves in a Beeler-Reuter based model of two-dimensional cardiac conduction. *Int. J. Bifurcat. Chaos.* **1**:431–444.
16. Qu, Z., Xie, F., Garfinkel, A., and Weiss, J.N. 2000. Origins of spiral wave meander and breakup in a two-dimensional cardiac tissue model. *Ann. Biomed. Eng.* **28**:755–771.
17. Fenton, F., and Karma, A. 1998. Vortex dynamics in three-dimensional continuous myocardium with fiber rotation: filament instability and fibrillation. *Chaos.* **8**:20–47.
18. Rappel, W.J. 2001. Filament instability and rotational tissue anisotropy: a numerical study using detailed cardiac models. *Chaos.* **11**:71–80.
19. Luo, C.H., and Rudy, Y. 1991. A model of the ventricular cardiac action potential: depolarization, repolarization, and their interaction. *Circ. Res.* **68**:1501–1526.
20. Allessie, M.A., Bonke, F.I.M., and Schopman, F.J.C. 1973. Circus movement in rabbit atrial muscle as a mechanism of tachycardia. *Circ. Res.* **33**:54–77.
21. Pertsov, A.M., Davidenko, J.M., Salomonsz, R., Baxter, W.T., and Jalife, J. 1993. Spiral waves of excitation underlie reentrant activity in isolated cardiac muscle. *Circ. Res.* **72**:631–650.
22. Qu, Z., Weiss, J.N., and Garfinkel, A. 1999. Cardiac electrical restitution properties and stability of reentrant spiral waves: a simulation study. *Am. J. Physiol.* **276**:H269–H283.
23. Hilborn, R.C. 2000. *Chaos and nonlinear dynamics.* 2nd edition. Oxford University Press. New York, New York, USA. 650 pp.
24. Kim, Y.H., et al. 1999. Role of papillary muscle in the generation and maintenance of reentry during ventricular tachycardia and fibrillation in isolated swine right ventricle. *Circulation.* **100**:1450–1459.
25. Weiss, J.N., Garfinkel, A., and Chen, P.S. 2003. Novel approaches to identifying antiarrhythmic drugs. *Trends Cardiovasc. Med.* **13**:326–330.
26. Gilmour, R.F., Jr. 2003. A novel approach to identifying antiarrhythmic drug targets. *Drug Discov. Today.* **8**:162–167.
27. Wu, T.J., Lin, S.F., Weiss, J.N., Ting, C.T., and Chen, P.S. 2002. Two types of ventricular fibrillation in isolated rabbit hearts: importance of excitability and action potential duration restitution. *Circulation.* **106**:1859–1866.
28. Courtemanche, M. 1996. Complex spiral wave dynamics in a spatially distributed model of cardiac electrical activity. *Chaos.* **6**:579–600.
29. Fox, J.J., Bodenschatz, E., and Gilmour, R.F., Jr. 2002. Period-doubling instability and memory in cardiac tissue. *Phys. Rev. Lett.* **89**:138101-1–138101-4.
30. Chudin, E., Goldhaber, J., Garfinkel, A., Weiss, J., and Kogan, B. 1999. Intracellular Ca(2+) dynamics and the stability of ventricular tachycardia. *Biophys. J.* **77**:2930–2941.
31. Wu, Y., and Clusin, W.T. 1997. Calcium transient alternans in blood-perfused ischemic hearts: observations with fluorescent indicator fura red. *Am. J. Physiol.* **273**:H2161–H2169.
32. Boyden, P.A., and ter Keurs, H.E. 2001. Reverse excitation-contraction coupling: Ca2+ ions as initiators of arrhythmias. *J. Cardiovasc. Electrophysiol.* **12**:382–385.
33. Akar, F.G., and Rosenbaum, D.S. 2003. Transmural electrophysiological heterogeneities underlying arrhythmogenesis in heart failure. *Circ. Res.* **93**:638–645.
34. Davey, P., Bryant, S., and Hart, G. 2001. Rate-dependent electrical, contractile and restitution properties of isolated left ventricular myocytes in guinea-pig hypertrophy. *Acta Physiol. Scand.* **171**:17–28.
35. Taggart, P., et al. 2003. Effect of adrenergic stimulation on action potential duration restitution in humans. *Circulation.* **107**:285–289.
36. Yue, D.T., Herzig, S., and Marban, E. 1990. Beta-adrenergic stimulation of calcium channels occurs by potentiation of high-activity gating modes. *Proc. Natl. Acad. Sci. U. S. A.* **87**:753–757.
37. London, B., et al. 1998. Long QT and ventricular arrhythmias in transgenic mice expressing the N terminus and first transmembrane segment of a voltage-gated potassium channel. *Proc. Natl. Acad. Sci.*

U. S. A. **95**:2926–2931.
38. Nuyens, D., et al. 2001. Abrupt rate accelerations or premature beats cause life-threatening arrhythmias in mice with long-QT3 syndrome. *Nat. Med.* **7**:1021–1027.
39. Yamauchi, S., et al. 2002. Restitution properties and occurrence of ventricular arrhythmia in LQT2 type of long QT syndrome. *J. Cardiovasc. Electrophysiol.* **13**:910–914.
40. Walker, M.L., Wan, X., Kirsch, G.E., and Rosenbaum, D.S. 2003. Hysteresis effect implicates calcium cycling as a mechanism of repolarization alternans. *Circulation.* **108**:2704–2709.
41. Xu, A.X., and Guevara, M.R. 1998. Two forms of spiral-wave reentry in an ionic model of ischemic ventricular myocardium. *Chaos.* **8**:157–174.
42. LeGrice, I.J., et al. 1995. Laminar structure of the heart: ventricular myocyte arrangement and connective tissue architecture in the dog. *Am. J. Physiol.* **269**:H571–H582.
43. Hooks, D.A., et al. 2002. Cardiac microstructure: implications for electrical propagation and defibrillation in the heart. *Circ. Res.* **91**:331–338.
44. Qu, Z.L., Xie, F.G., and Garfinkel, A. 1999. Diffusion-induced vortex filament instability in 3-dimensional excitable media. *Phys. Rev. Lett.* **83**:2668–2671.
45. Munuzuri, A.P., et al. 1994. Elastic excitable medium. *Phys. Rev. E Stat. Phys. Plasmas Fluids Relat. Interdiscip. Topics.* **50**:R667–R670.
46. Vetter, F.J., and McCulloch, A.D. 2001. Mechano-electric feedback in a model of the passively inflated left ventricle. *Ann. Biomed. Eng.* **29**:414–426.
47. Antzelevitch, C., et al. 1991. Heterogeneity within the ventricular wall. Electrophysiology and pharmacology of epicardial, endocardial, and M cells. *Circ. Res.* **69**:1427–1449.
48. Lukas, A., and Antzelevitch, C. 1996. Phase 2 reentry as a mechanism of initiation of circus movement reentry in canine epicardium exposed to simulated ischemia. *Cardiovasc. Res.* **32**:593–603.
49. Janse, M., and Kleber, A. 1982. Electrophysiological changes and ventricular arrhythmias in the early phase of regional myocardial ischemia. *Circ. Res.* **49**:1070–1081.
50. Weiss, J.N., Chen, P.S., Qu, Z.L., Karagueuzian, H.S., and Garfinkel, A. 2000. Ventricular fibrillation. How do we stop the waves from breaking? *Circ. Res.* **87**:1103–1107.